Robust Identification and Residual Generation Application to a Turbofan Engine

Andrés Marcos, Gary J. Balas
Department of Aerospace Engineering and Mechanics
University of Minnesota,
107 Akerman Hall, 110 Union St. SE, Minneapolis
fax: +1 612 626-1558
e-mails: marcosa@aem.umn.edu,
balas@aem.umn.edu

Dinkar Mylaraswamy
Honeywell International Inc.,
3660 Technology Drive
Minneapolis, MN 55418, USA
fax: +1 612 951-7438
e-mail: dmylaras@honeywell.com

Abstract— In this paper we describe an application of a model-based fault detection and isolation technique to a turbofan aircraft engine. Our approach is based in $\mathcal{H}_\infty$-optimization, a frequency domain technique that explicitly addresses robustness. The engine model is obtained through a robust identification approach combining the classical time-data system identification via prediction error models and the so-called model error model theory. The time-data series are provided by one of Honeywell's airline customers. The model error model approach provides guidelines for the characterization of the model uncertainty stemming from the nominal system identification. The $\mathcal{H}_\infty$ filter is used to detect faults in the engine's high-pressure turbine while minimizing disturbances and commands effects.

1. INTRODUCTION

A driving economic force in the aerospace industry, particularly commercial airlines, is the use of aircraft engine anomaly and fault detection schemes to improve their reliability and optimize (reduce) their maintenance schedules. The main goal is to utilize trending and fault detection & isolation (FDI) algorithms to reduce the false alarm rate while maintaining the high level of safety required for their safe operation. This reduction in false alarms has a great economic impact since by reducing the number of times an engine has to be serviced it increases the operational capability of the air fleet and reduces the maintenance costs. This interest has resulted in a great number of publications related to fault detection and identification for jet engines covering analytical redundancy [18] for both data-driven [26], [7] and model-based approaches [9], [10].

The most widespread approach to on-line fault detection is based in the voting schemes arising from hardware redundancy. The drawback of these approaches is the cost incurred in this hardware duplication. Analytical redundancy approaches reduce the required hardware by providing redundant information based on reference models or dissimilar systems. A form of analytical redundancy is provided by neural networks (NN), which can be used to obtain nominal and faulty non-linear models from data training sets— effectively combining the model identification stage with the residual generation algorithm [12]. The success of these NN-based approaches is based on the availability of numerous sets of data to adequately train the network, which is quite difficult for the fault case. Model-based approaches provide analytical redundancy using a mathematical model of the system obtained also by system identification or first order principles. These approaches might suffer robustness problems due to the ideal approximations used to obtain this reference model. Among the latter approaches, $\mathcal{H}_\infty$ optimization-based algorithms are of great interest due to their explicit incorporation of robustness [11], [20]. From an off-line perspective, the current state-of-the-art in the industry involves empirical (neural networks, clustering [26], [12]) and model-based techniques (least-squares estimation [9]).

In this paper we present an application of $\mathcal{H}_\infty$-optimization to fault detection for a Honeywell turbofan engine. The application combines parametric identification, uncertainty characterization, and FDI. The engine model is obtained by applying prediction error model identification algorithms [14] to a set of engine flight data provided by a Honeywell airline customer. The bias error, or model uncertainty, arising from the nominal system identification is initially characterized by the model error model approach [13]. This combination of nominal and model error model identification, considered a robust model identification approach [13], [21], fits naturally in the robust fault detection and isolation framework of $\mathcal{H}_\infty$-based algorithms. The goal of the FDI filter is to identify incipient and abrupt faults during the cruise regime on the high-pressure turbine (HPT) (a parametric fault), minimizing the effect of the disturbances and commands on the residual while providing robustness to modelling uncertainty. Note that although the identified LTI model is quite good for time simulations there is some frequency mismatch that adversely affect the performance of the FDI filter. Work is being done to obtain more accurate frequency models.

The paper is organized into seven sections, the first being this Introduction. The second section provides a theoretical review of the robust system identification and the robust residual generation algorithms used in this paper. The third section

0-7803-8155-6/04/$17.00/
IEEEAC paper # 1472

introduces the turbofan engine model and the fault to be identified. Section 4 presents the nominal linear time invariant (LTI) model identification results. Section 5 gives the results for the robust identification algorithm. Section 6, formulates the robust residual generation problem applied to the turbofan engine and provides the simulation results. Conclusions are given in Section 7.

2. THEORY

The approach followed in this paper uses a three step algorithm: i) nominal model identification, ii) robust identification, and iii) the proper robust residual generation approach. These steps are reviewed in detail below.

Nominal Model Identification

In the control field system identification is understood to be a process by which a dynamic model is obtained from measured input and output data. The identified model is selected from a family of models and is described by a finite set of parameters and a structure (the relation between the parameters). To obtain a good and reliable model, the designer must pay attention to several aspects, including the choice of an appropriate input/output data set, selection of the model structure and order, and thorough validation of the resulting model [14], [15].

The selection of the model structure is the most important step in any system identification procedure. Non-parametric models (correlation and frequency response models) give insight into the physical behavior of the model, its temporal character, and its frequency content by signaling regions of interest. Unfortunately, these non-parametric models might not provide a high-degree of accuracy, hence parametric models are selected in this paper for the structural identification stage (and the non-parametric models are used as analysis tools to gain insight on the engine model). Equation (1) formulates the most general type of black-box parametric structure:

$$A(q)y(t) = \frac{B(q)}{F(q)}u(t-nk) + \frac{C(q)}{D(q)}e(t) \tag{1}$$

where the polynomials are given by

$$A(q) = 1 + a_1 q^{-1} + \ldots + a_{na} q^{-na} \tag{2}$$

$$B(q) = b_1 + b_2 q^{-1} + \ldots + b_{nb} q^{-nb+1} \tag{3}$$

$$C(q) = 1 + c_1 q^{-1} + \ldots + c_{nc} q^{-nc} \tag{4}$$

$$D(q) = 1 + d_1 q^{-1} + \ldots + d_{nd} q^{-nd} \tag{5}$$

$$F(q) = 1 + f_1 q^{-1} + \ldots + f_{nf} q^{-nf} \tag{6}$$

The nominal identification algorithm used in this report is based in a *model-batch* evaluation approach: a set of candidate structures are selected and then evaluated using different orders and delays [15]. The three main model structures chosen are: auto-regressive with exogenous input (ARX), output error (OE), and a general predictive model (PEM). Continuous-time, closed-loop engine data provided by a partner airline in Honeywell's Predictive Trend Monitoring (PTM) project is used for identification purposes.

Model Error Model Identification

In system identification the estimation of a suitable model with an appropriate uncertainty description has been addressed mostly through the so called "robust control-oriented" identification [13], [8]. This is closely related to the robust model validation theory [23], [13] .

The concept of the model error model (MEM) introduced in reference [13] allows a very defined separation of the residual into bias (modeling uncertainty) and variance (noise error) errors. The model error model provides as well with an alternative test to the classical residual validation approach. In references [16], [21] this MEM concept is used to provide frequency-domain characterizations of the model uncertainty for the purposes of control-oriented model validation. The approach used in those references provide a natural fit with the robust control design framework. In this paper, this natural fit is used in the robust fault detection and isolation framework by using the model error model as an initial uncertainty weight.

There are no restrictions on the identification approach used for the nominal model or the model error model. Furthermore, the identification of the latter is not affected by the method or assumptions used to obtain the nominal model. The only information required for MEM identification is the residual estimates $\varepsilon(t)$ obtained using a (possibly different) set of output/input measurements. An algorithm and guidelines to calculate the model error models for an identified nominal system can be found in [13], [22], [21].

As suggested in reference [21], a simple approach to calculate an additive uncertainty weight from the uncertainty regions obtained using the nominal and MEM models is simply to calculate the lower error bound $\gamma(i\omega)$ that bounds the uncertainty region, $\Delta_a(i\omega)$, such that $\{G_o(i\omega) + \Delta_a(i\omega) \mid \Delta_a(i\omega \leq \gamma(i\omega)\}$. Constant and first-order approximations are recommended to decrease the total order of the $\mathcal{H}_\infty$ FDI filter to be synthesized later.

Robust Residual Generation

The problem of designing a robust $\mathcal{H}_\infty$ fault detection and isolation filter is generally divided in two main stages: first, a robust residual generation and second, a robust residual evaluation (see references [5], [3] for example). We will focus on the first task: how to design a robust residual generator using $\mathcal{H}_\infty$ optimization techniques. Within the task of residual generation, and from the $\mathcal{H}_\infty$ perspective, the design problem can be divided in two parts: i) transforming the problem into the standard $\mathcal{H}_\infty$ formulation [27], [24] and ii) defining the appropriate optimization index. Weight selection is also an integral

part of a correct and meaningful solution to the problem.

Assume a generalized plant with no-uncertainty is available (actuators, sensors, and weighting functions are embedded in the plant description):

$$y(s) = G_u(s)u(s) + G_f(s)f(s) + G_d(s)d(s) \tag{7}$$

The transfer function $G_u(s)$ determines the effects on the system of the known inputs, $u(s) \in \mathcal{R}^{n_u}$; those from the faults, $f(s) \in \mathcal{R}^{n_f}$, are given by $G_f(s)$, and $G_d(s)$ refers to those from the disturbances $d(s) \in \mathcal{R}^{n_d}$. These transfer functions are assumed to be known. A general residual generator F with post-filter transfer function Q is given by:

$$\begin{aligned} r(s) =& F[u^\top \; y^\top]^\top = Q(s)[H_u(s)u(s) + H_y(s)y(s)] \\ =& Q(s)[G_f(s)f(s) + G_d(s)d(s)] \end{aligned} \tag{8}$$

Note that to obtain Equation (8) we have to make use of the standard residual generator condition, i.e. $H_u(s) + H_y(s) \cdot G_u s = 0$. The filter F needs to cancel or minimize the effect of the disturbances, $min \mid\mid G_{d \to res} \mid\mid_\infty$, while maximizing the effect of the faults on the residual, i.e. $max \mid\mid G_{f \to res} \mid\mid_\infty$. This multi-objective optimization is not easily amenable to $\mathcal{H}_\infty$ techniques due to its min-max characteristics.

To adequately estimate the faults, an ideal fault model $T_{f_{id}}$ in the spirit of the model-matching approach can be used, see [3], [4]. Typically, this reference model is diagonal for fault de-coupling purposes (isolability) and, depending on the type of application, it can be an identity matrix [25] or a frequency dependent weight used to emphasized the frequency band of interest [6], [19]. This ideal model also allows for a more proper blending of the optimization objectives. Maximizing the effect of the faults on the residual is transformed into minimizing the error between the residual and the weighted fault, i.e $max \mid\mid G_{f \to e} \mid\mid_\infty \equiv min \mid\mid res - T_{f_{id}} \cdot f \mid\mid_\infty$. Hence the optimization index becomes a standard minimization of the transfer function from fault and disturbances to the error.

From robust control theory the concept of *uncertainty balls*, in the Nyquist sense, can be used to define model uncertainty: $\mathcal{B}_\Delta := \{ \Delta(s) \in \mathcal{RH}_\infty \mid \| \Delta \|_\infty < \gamma \}$ where γ defines a level of uncertainty. In reference [3] a general residual generator is obtained under the assumption that all the system transfer functions have multiplicative uncertainty. The input-output representation of such a system is given by:

$$\begin{aligned} y =& G_u(I + \Delta_u)u + G_f(I + \Delta_f)f + G_d(I + \Delta_d)d \\ =& G_u u + G_f f + G_d d + G_u \Delta_u u + G_f \Delta_f f + G_d \Delta_d d \end{aligned} \tag{9}$$

Note that the uncertainty model can be represented by a general (possibly more conservative) additive model:

$$y = G_u u + G_f f + G_d d + \tilde{\Delta}_u u + \tilde{\Delta}_f f + \tilde{\Delta}_d d \tag{10}$$

Figure 1 shows the standard $\mathcal{H}_\infty$ filter problem with structured uncertainty.

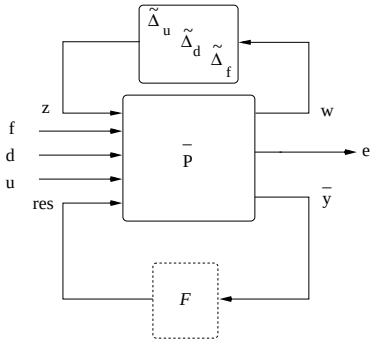

Figure 1. Standard $\mathcal{H}_\infty$ robust fault diagnosis problem.

Assume that all the uncertainty descriptions have been lumped into a (structured or unstructured) uncertainty set characterized by $z = \Delta \cdot w$. The perturbation output z can be considered as a special type of disturbance (see reference [2]) and combined with the disturbance d to form a generalized disturbance vector, $\bar{d} = [\, z^\top \; d^\top \,]^\top$. The $\mathcal{H}_\infty$ **robust fault diagnosis problem** is then defined as finding a stable filter F such that the performance error is minimized in the face of all the possible uncertainties defined by $||\Delta|| \leq 1$.

3. Turbofan Engine Model

The turbofan engine under consideration is a two-spool, high bypass engine. The engine is composed of four major modules which can be serviced separately for ease of maintenance and repair. These modules are the fan section, the gas producer module, the combustor/turbine module and the accessory gearbox section. The engine modules can be grouped into two major systems depending on the type of pressure they use (high or low).

The low pressure system is composed (from front to rear) by a single stage fan connected to a two-stage compressor, also known as super-charger, and both mounted on a fan shaft. The system is driven by a two-stage turbine which transmits the mechanical energy required to move the system by means of a turbine rotor assembly shaft. Since the fan requires a lower r.p.m., a single stage sun/planetary gear arrangement connects the fan shaft and the turbine rotor shaft to reduce the revolutions of the latter.

The high pressure system of the engine is a more complex mechanical system; it is formed by a combination of an axial and a centrifugal compressor. The two compressors are mounted on a single shaft connected to a two-stage turbine. This high pressure shaft encircles the low pressure turbine rotor shaft in a co-annular fashion. An accessory gearbox is located at the front of the compressor and provides with the rotational energy for all engine driven devices.

For purposes of this project, a (dynamic, open-loop, black-

box) nonlinear simulation model is available together with engine continuous-time closed-loop data. The simulation model has four main inputs: the first three can be considered as *disturbances* (total air temperature, *TAT* Celsius, Mach number *Mn*, and pressure altitude, *Alt* feet), and the fourth input is the command signal (fuel flow, Wf lbs/hr). There are three output channels: fan speed $N1$ in % r.p.m, high-pressure (core) speed $N2$ % r.p.m., and exhaust gas temperature EGT in Celsius. An electronic control unit (ECU) regulates the amount of fuel flow used to control the fan speed by means of regulation of $N2$.

Additional input channels to the simulation model account for faults and aircraft/engine bleed. The bleed channels can only have two positions: close (no bleed) or open (bleed). The main bleed channels are the engine's anti-ice system and the system bleed air (used to feed bleed air to most of the aircraft and engine systems). There are six possible *fault* channels but only the first fault, HPT_f, is considered. This fault channel characterizes a high pressure turbine (HPT) deterioration due to leading edge erosion or tip clearance change (i.e. distance between the turbine blades and the turbine encasing). It is measured as a dimensionless number.

4. Nominal Model Identification

This section describes the identification results for the nominal model and the fault model. The algorithm presented in Section 2 is used to identify an LTI Multiple-Input-Multiple-Output (MIMO) nominal model for the LF507-F1 engine using continuous-time data series. This nominal MIMO model is augmented by a MIMO model characterizing the HPT_f fault effects on the engine outputs.

The operational envelope of interest is the cruise flight regime, hence the signals for identification and validation are obtained by combining four different cruise data sets for each signal. Figure 2 shows the input data for the identification signal.

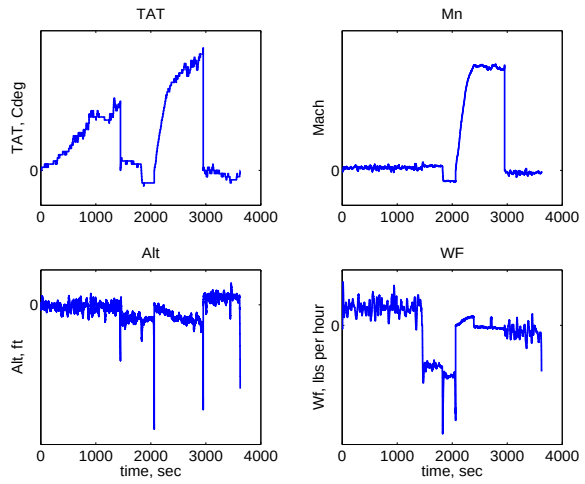

Figure 2. Identification Signal Input Data.

The large deflections observed are mainly the product of the data sets' connection. If these discontinuities were to be considered too severe for the identification, the data could be prefiltered. In the present case, the discontinuities are left to artificially introduce some nonlinear behavior that might arise from sudden reduction of speed during the cruise regime (i.e. the pilot can always maintain altitude while reducing speed by using the inter-play between the thrust and the elevators). Figure 3 shows the fan speed $N1$ output time history for the identification signal.

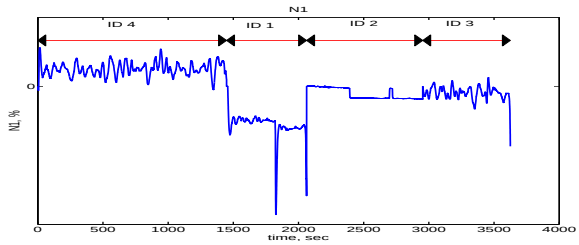

Figure 3. Identification Signal Output Data, $N1$.

As mentioned in Section 2, three prediction error models are used: ARX, OE and PEM. Different orders and delays are tested until a satisfactory model is obtained. A primary concern is to obtain relatively low-order models since this influences the final order of the $\mathcal{H}_\infty$ FDI filter. The criterion for fit is a combination of quantitative and qualitative measures. There are three quantitative measures used: the Akaike's Information Theoretic Criterion (AIC) and Final Prediction Error (FPE), and the percentage of output variation explained by the model simulation (PCT) [14]. Together with these criteria, the classical residual analysis, time-domain comparisons, and frequency-domain estimation, i.e. empirical transfer functions (ETFE) and spectral estimate (SPA), are used to qualitatively evaluate the models.

Nominal Model Identification Results

This subsection presents the identification of the fault-free Multiple-Input-Single-Output (MISO) models, one model per output, using engine data obtained from the Predictive Trend Monitoring (PTM) database. The identification is restricted to the cruise flight regime. The inputs for all the models are the engine disturbance inputs (TAT,Mn, and Alt) and the control engine input (Wf). The outputs for each of the three models are $N1$, $N2$ and EGT respectively.

Table 1 shows the structure, order of the coefficients, and delays for each of the MISO models. The terminology follows that of reference [17]. Numbers within brackets indicate the order of the four input channels for that coefficient (a single number means all channels have the same order), see also Equation (1).

For the ARX model, a bandpass Butterworth filter with a frequency band of $[10e^{-5}\ \ 0.5]$ rad/s is used to focus in the low-mid frequency region. An example of the quantitative results

Table 1. Structural nominal LTI MISO models.

Model	Struc.	na	nb	nc	nd	nf	nk
MISO $N1$	OE	0	[1]	0	0	[1]	[0]
MISO $N2$	ARX	5	[5]	0	0	[0]	[0]
MISO EGT	OE	0	[1]	0	0	[1]	[1]

obtained is given by the fit criteria for the MISO $N1$ model using the identification signal: $FPE = 1.90873e^{-01}, AIC = -1.65614$, and $PCT = 90.53235$ %, which indicates a very good fit. Similar results (with a minimum $PCT \approx 80\%$) are obtained for the other two models.

Figure 4 provides the time simulation comparison between the measured validation signal (solid) and the simulated output (dashed) for the MISO $N2$ model. The plot shows good agreement. Similar results are obtained for the other models with the EGT model showing some level of bias.

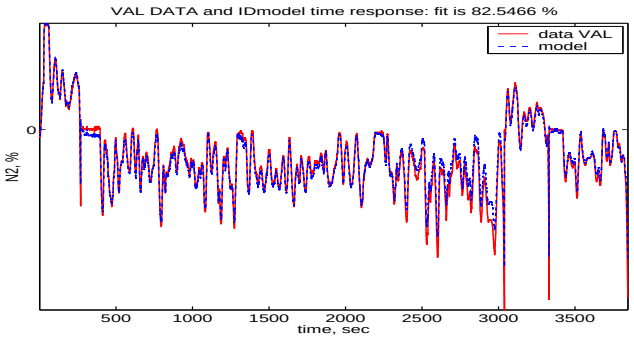

Figure 4. VAL signal time response comparison, MISO $N2$.

Figure 5 shows the frequency response comparison (i.e. ETFE, SPA obtained from the data and that for the identified model) for the MISO $N2$ model. One of the qualitative criteria is to obtain acceptable fit for the low-mid frequency region. The ETFE shows a large phase discrepancy around the one radian region. This discrepancy will have undesirable consequences on the achievable robustness of the diagnosis filter designed with this model.

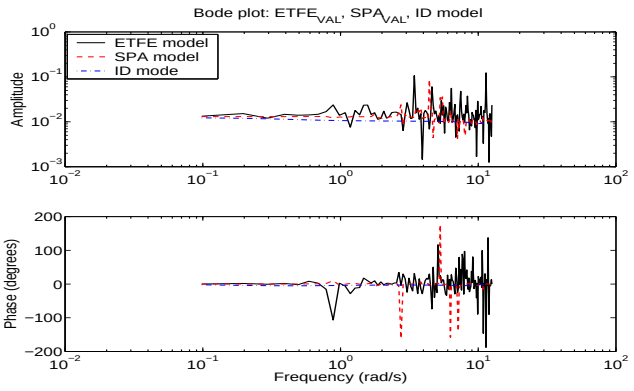

Figure 5. Frequency analysis comparisons, MISO $N2$.

The classical residual analysis is given in Figure 6 for the MISO EGT model. It shows that the model is not falsified (the auto-correlation is not meaningful in this case since it is an output error model [14]). The figure shows the auto and cross-correlation (w.r.t. the TAT input channel) for the MISO EGT using the validation signal. With respect to the other models and signals, the MISO $N1$ model shows falsification by the validation signal while the rest pass the residual test with only occasional small cross-correlation in the first few lags for the Alt and Wf channels.

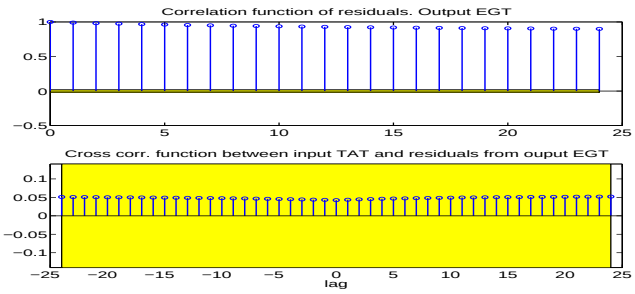

Figure 6. Auto and cross-correlation, MISO EGT.

Time simulations with forty-two different cruise flight data sets yielded acceptable comparisons. Nevertheless, the EGT channel presents a larger bias—probably caused by control feedback in the data. This bias can be seen in Table 2, which gives the mean (MEAN) and standard deviation (STD) between the simulated LTI MIMO model, formed by the augmentation of the three MISO models, and the data for all the flights.

Table 2. Statistical properties for 50 cruise flights.

	N1	N2	EGT
MEAN	0.03004	0.02706	1.98002
STD	0.15655	0.04701	2.28696

In summary, a 13 order LTI nominal engine MIMO model is identified with good time-domain and acceptable frequency-domain fits but with some cross-correlation problems. Information regarding the falsification of the models should be obtained to account for this falsification in the robust residual generation stage. This information can be obtained, together with an alternative residual test, using the model error model concept, see Section 5.

Fault Model Identification Results

In this subsection an identification similar to that for the nominal model above is used to obtain an LTI model of the HPT fault effects. Since no faulty data sets are identified, the engine simulation model is used in combination with flight data sets to obtain the required input/output faulty measurements. A MISO identification is also performed. SISO identifications yielded higher order models for the same level of performance.

The identification and validation signals are each formed by using a different flight data set and a different 'pure' fault signal injected in the simulation model. The fault signals are selected to be an initial ramp followed by a pseudo-random binary signal (PRBS) in order to represent the slow degradation of the fault followed by abrupt breakage (i.e. incipient and abrupt faults). The PRBS is used to provide the identification with appropriate dynamic and magnitude information of the possible faults. Figure 7 shows the 'pure' fault signal used for identification.

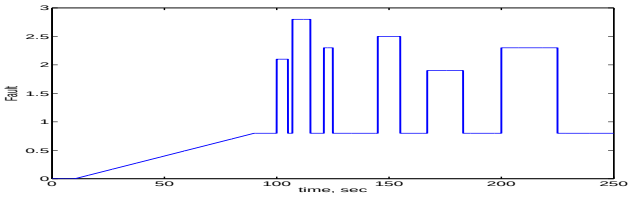

Figure 7. Fault identification signal.

The same identification procedure as for the nominal model is followed except that only ARX and OE models are tested. Table 3 shows the final order and structure selected. Note that in this case, there are five input channels: the previous four plus the fault input.

Table 3. Structural fault LTI MISO models.

Model	Struc.	na	nb	nf	nk
MISO $N1$	OE	0	[1 1 1 2 2]	[1 1 1 2 2]	[0]
MISO $N2$	ARX	1	[1]	[0]	[0]
MISO EGT	ARX	1	[1]	[0]	[0]

Good time simulation comparisons are obtained for the identified fault models, Figure 8 shows the most divergent case (i.e. the fault validation signal for the fault MISO $N2$ model). The plot shows the residual formed by subtracting the no-fault case for the same flight data, i.e. it shows only the fault effects.

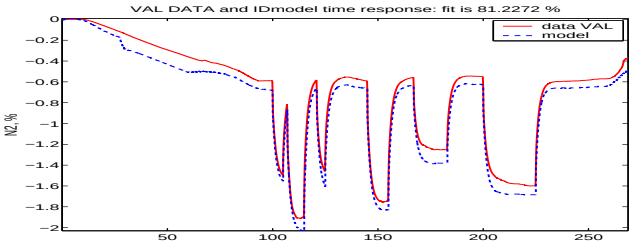

Figure 8. Time response comparison, MISO HPT_f to $N2$.

As before, frequency and residual analyses were performed. It is desirable as well to obtain good fit for the low-mid frequency region while no emphasis is placed on the residual tests. The reason for not placing emphasis on residual tests is that closed-loop flight data and a designed fault signal are injected in an open-loop model (hence, we expect high levels of correlation between inputs).

The LTI MIMO fault model identified has nine states and, when augmented with the nominal MIMO model, good nominal and fault time simulations are obtained.

5. Robust Model Identification

In this subsection, we present the model error models (MEM) associated with the nominal models identified in the previous section. One MEM exists for each of the identified MISO nominal models (i.e. a total of three models corresponding to the number of outputs in the system). As established earlier, the purpose of these model error models is to provide an alternative test to the classical residual validation; it also provides initial characterizations of the model uncertainty for the application of the robust residual generation algorithm.

Model Error Model

Model error models should be more flexible than the identified model on which they are based in order to capture the possible non-linearities and dynamics that are not adequately represented by the nominal model. A Box-Jenkins general parametric model provides this flexibility of design. Furthermore, due to the closed-loop nature of the data and the interdependencies of the inputs, a MISO identification is used. A SISO identification using the fuel flow as the driving input was also tried with much less success. The same identification and validation signals applied to the previous nominal model identification (see Section 4) are used to identify the MEMs.

Table 4 shows the order of the coefficients and delays for each of the MISO MEM models. The differences among the orders of the input channels for the same MEM are immediately noticeable. These differences illustrate the more difficult task that the MEM identification presents. Indeed the ouput percentage fit is around 20 % for most of the validation signals tested.

Table 4. Structural LTI MISO model error models.

Model	na	nb	nc	nd	nf	nk
MEM $N1$	0	[2 5 3 2]	4	4	[5 5 5 5]	[2 2 0 2]
MEM $N2$	0	[1 1 1 4]	1	1	[4 4 4 4]	[2 1 2 1]
MEM EGT	0	[1 1 1 4]	2	2	[1 1 1 4]	[1 1 1 0]

Figure 9 shows the Mn and Alt cross-correlation for the EGT MEM model using the validation signal. The case shown marginally satisfies the residual test for three standard deviations, but it is also the worst case obtained. The other channels and models pass the test with some cross-correlation stemming from Wf for the validation signal.

Now we turn our attention to the alternative nominal model validation test that the model error model provides. In Section 4 it was noted that the residual test was not passed for the validation signal and the nominal MISO $N1$ model, and some initial cross-correlation issues were also identified in the Alt, WF channels for the other models. References [13],

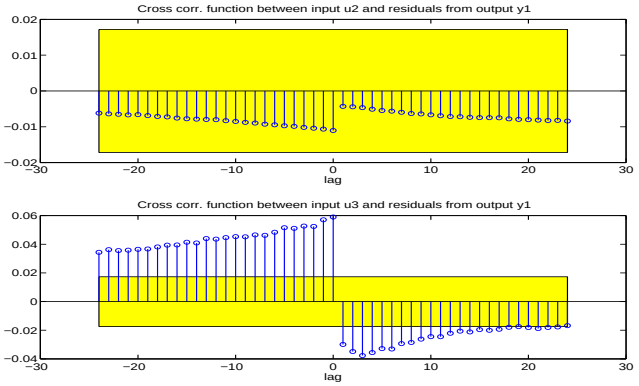

Figure 9. Auto and cross-correlation, MEM EGT.

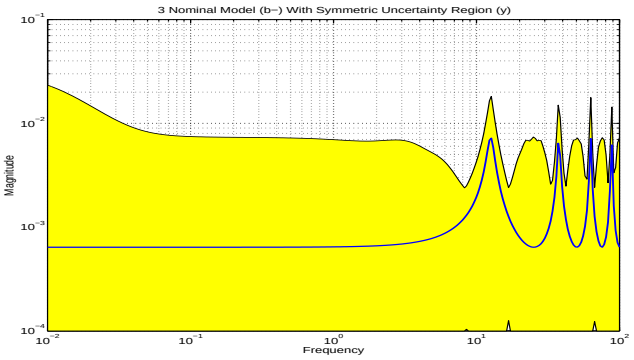

Figure 11. Symmetric uncertainty region, MEM $N1$ channel Alt.

[21] mention that the falsified nominal model is still of use if additional information with respect to the uncertainty is obtained. In Figure 10, the non-symmetric region (shade) and the nominal model (solid line) for the $N1$ model, specifically the Alt channel, is shown. It is clear that the nominal model is falsified since it is not completely included within the uncertainty region. Indeed, this happens for the Alt and Mn of all the models (except the Alt channel in the EGT model) which seems to indicate this test is more stringent than the classical residual test. The conclusion is that care should be exercised for these two channels at frequency regions approximately between $[0.03 \rightarrow 10]$ radians for the robust residual generation. Furthermore, for the $N2$ model, as was noted earlier, large phase discrepancies occur around the one radian region, see Figure 5. The MEM uncertainty characterization reflected this by using larger peaks of the uncertainty frequency band around the $[1 \rightarrow 15]$ radians region (specially in the Mn channel). This also highlights a limitation of the MEM uncertainty characterization whereby phase information is only indirectly considered in the definition of the uncertainty bands.

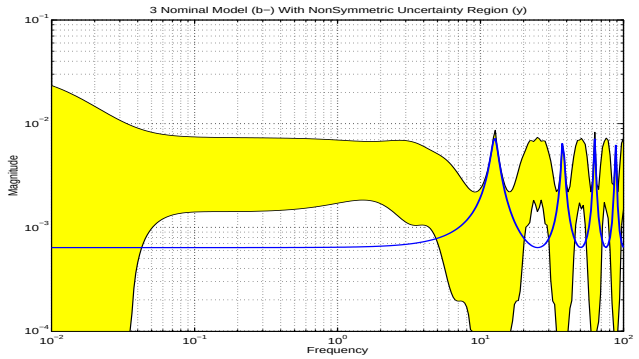

Figure 10. Non-Symmetric uncertainty region, MEM $N1$ channel Alt.

Figure 11 provides the symmetric region for the same model and channel. As expected by design, the previous uncertainty region and the nominal model are included. This region is more conservative than the previous one, but it can now be used for uncertainty modeling in the frequency region.

Uncertainty Characterization

As discussed in Section 2, additive uncertainty weights are calculated for the uncertainty regions. The $\mathcal{H}_\infty$-norm of the uncertainty region is used to obtain constant bounds for some of the channels, while first order fits (obtained using the command *drawmag* from [1]) are used for some other channels. These weights are used in the robust residual generation stage as an initial characterization of the uncertainty. Figures 12 and 13 provide an example of a constant and a first order fit for the fuel flow channel of the $N2$ and EGT models respectively.

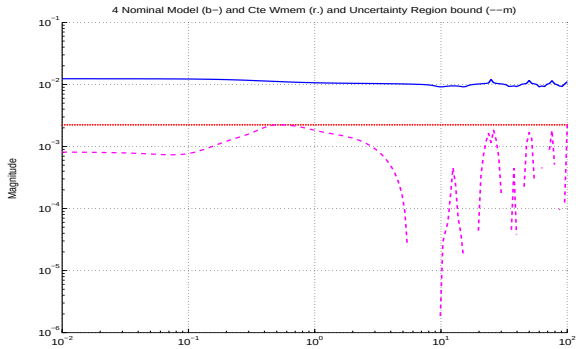

Figure 12. Constant fit symmetric uncertainty region, MEM $N2$ channel Wf.

6. Robust Residual Generation

In this section the robust residual generation algorithm presented earlier is used to detect and isolate high pressure turbine faults HPT_f. The approach is divided in two major steps: first, the formulation of the problem (exemplified by the $\mathcal{H}_\infty$ interconnection), and second, the weight design.

Problem Formulation

The problem uses an ideal fault model $T_{f_{id}}$ reference tracking approach as shown in Figure 14. Additive uncertainty weights $\Delta_a W_a$ are used to account for robustness. Noise weights W_n and performance weights W_e are also used to for-

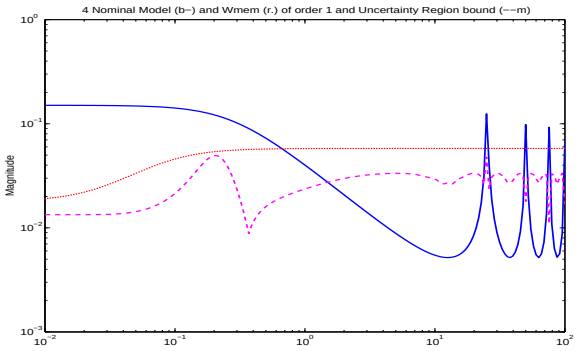

Figure 13. First order fit symmetric uncertainty region, MEM EGT channel Wf.

mulate the problem. The plant G, given by Equation (7), is the augmented (nominal and fault) MIMO LTI model from Section 4.

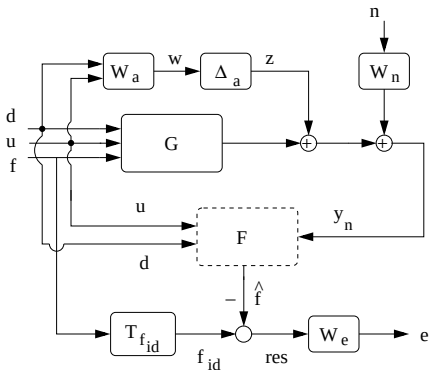

Figure 14. $\mathcal{H}_\infty$ interconnection LF-507-F1.

The exogenous disturbance vector is given by $d = [TAT, Mn, Alt]^\top$ and the noise by $n = [N1, N2, EGT]^\top$. The fuel flow command is represented by u, the HPT_f fault by f, and the weighted performance error by e. Lumping all the inputs to the interconnection together, i.e. $\tilde{d} = [n^\top\ d^\top\ u^\top\ f^\top]^\top$, the robust FDI $\mathcal{H}_\infty$ problem is given by:

$$\begin{aligned} &\min \| TF_{\tilde{d}\to e} \|_\infty \\ &\text{subject to } |\Delta_a| \le 1 \end{aligned} \tag{11}$$

Notice that this interconnection uses the disturbances also as direct inputs to the filter. These disturbance channels are measurable and their introduction to the filter provides additional information regarding plant variations and helps enforce the disturbance decoupling condition.

Writing out the relations that arise from the above interconnection, we obtain the following equations:

$$e = W_e(T_{f_{id}} f - I\ \hat{f}) \tag{12}$$

$$y_n = W_n n + G[d^\top u^\top f^\top]^\top + \Delta_a W_a [d^\top u^\top]^\top \tag{13}$$

$$\hat{f} = F(u + d + y_n) = F_u u + F_d d + F_y y_n \tag{14}$$

Combining the previous equations (together with Equation (7)) and noting that the objective is to minimize the resulting transfer function, the following five conditions are obtained:

$$W_e(T_{f_{id}} - F_y G_f) f = 0 \tag{15}$$

$$W_e F_y W_n n = 0 \tag{16}$$

$$W_e[F_d + F_y(\Delta_a W_{a_d} + G_d)]d = 0 \tag{17}$$

$$W_e[F_u + F_y(\Delta_a W_{a_u} + G_u)]u = 0 \tag{18}$$

The first condition, Equation (15), is the fault detection and isolation objective. The second and third conditions, Equation (16) and (17) respectively, provide the noise and disturbance rejection goals. The last condition, Equation (18), is used to enforce the command decoupling objectives.

Weight Design

From the *fault detection and isolation objective* in Equation (15), assuming an ideal situation, the following is obtained:

$$F_y = T_{f_{id}} G_f^{-1} \tag{19}$$

Since G_f (the fault effects on the model) is known and fixed, it only remains to specify the ideal fault model $T_{f_{id}}$. This reference model is typically designed from knowledge or assumptions on the fault behaviour. Additionally, since condition (15) should tend to zero, the ideal model and the error performance weight W_e must be designed together to satisfy the condition. These two weights are the main knobs the designer uses to define the bandwidth of the filter and its temporal characteristics (steady-state error, overshoot, and so on). In Figure 15, the frequency response of the nominal model for the fault effects G_f is shown. Notice the low-pass characteristics of the models and also the relative high DC gain for the EGT channel.

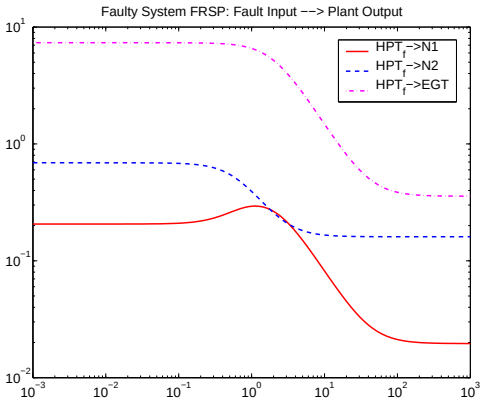

Figure 15. Frequency response fault to outputs.

To compensate for the effects of the inverse of G_f and provide adequate tracking of the fault at low-frequencies, a low-pass weight is used for the ideal fault model.

$$T_{f_{id}} = 9\frac{\frac{s}{10}+1}{\frac{s}{0.04}+1} \tag{20}$$

The bandwidth of the ideal model is selected to avoid coupling from the disturbances. This implies a detection time (i.e. rise time) of approximately 100 seconds. Faster (higher bandwidths) response can easily be obtained, though it compromises the disturbance rejection capabilities of the filter. Since the diagnosis filter is to be implemented off-line this slower response is considered acceptable.

The *noise rejection condition* plays a major role together with the first condition in shaping F_y, hence it should be defined also in conjunction with $T_{f_{id}}$. The error weight is also important to reduce the noise effects at those regions of interest. The W_n weights are typically chosen from knowledge of the system (i.e. MEM, covariance analysis, statistics, ...). For attitude and position sensor models the weights tend to be high-pass functions, while for accelerometers and process noise they are low-pass. They directly affect the minimization bound to be achieved and of course the noise level of rejection to be expected. In the present case they are selected as constant weights:

$$W_{n_{N1}} = W_{n_{N2}} = 2;\ W_{n_{EGT}} = 50 \tag{21}$$

The *command decoupling* condition, Equation (18), is analyzed next. This condition allows us to directly manipulate the effects of the command input on the filter, F_u:

$$W_e F_u = -W_e F_y(\Delta_a W_{a_u} + G_u) = -W_e F_y \hat{G}_u \tag{22}$$

The above equation indicates that F_u and $F_y\hat{G}_u$ should be approximately the same (in a magnitude sense). Furthermore, since F_y is mostly defined from the previous two conditions and G_u is fixed, the transfer function F_u is also almost defined. The additive uncertainty weights for the command inputs W_{a_u} are generally used to account for under-modelled high-frequency dynamics but can also be used to shape this condition. If necessary, it is possible to use W_e to minimize the effects of the term $[F_u + F_y(\Delta_a W_{a_u} + G_u)]$ at low-frequencies (the region of interest). Usually, the uncertainty weights are given by high-pass functions although to reduce the order of the filter (equal to the total number of states in the interconnection) constant weights can be chosen. Looking at the weighted transfer functions for the filter command channels, Figure 16, and guided by the MEM information the following weights are chosen. Note that u_1, u_2 and u_3 indicate the corresponding output ($N1, N2, EGT$ respectively), and the input channel is given by the sub-index (in this case the fuel flow command Wf):

$$Wu1_{Wf} = Wu2_{Wf} = \frac{1}{150};\ Wu3_{Wf} = \frac{1}{40}\frac{\frac{s}{0.5}+1}{\frac{s}{20}+1} \tag{23}$$

The *disturbance decoupling* objective is given by Equation (17):

$$W_e[F_d + F_y(\Delta_a W_{a_d} + G_d)] = 0 \tag{24}$$

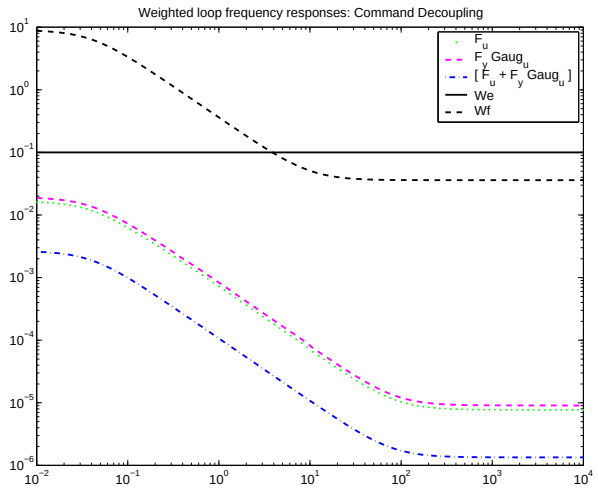

Figure 16. Weighted loops for the filter command term, F_u.

The inclusion of the disturbance channels to the filter provides a "direct" disturbance effects term on the filter, i.e. F_d, which can be used by the optimization to cancel the $F_y(\Delta_a W_{a_d} + G_d)$ term. As before, the F_y is shaped mainly by the noise and fault diagnosis conditions (Equations (16) and (15)). The disturbance effects on the plant G_d are also fixed. Hence, the disturbances additive uncertainty weights are used to incorporate robustness to the filter and shape this condition. Starting with the initial characterization obtained in Section 5 the weights given below are chosen.

$$Wu1_{TAT} = Wu2_{TAT} = \frac{1}{30};\ Wu3_{TAT} = \frac{1}{80} \tag{25}$$

$$Wu1_{Mn} = Wu2_{Mn} = \frac{1}{80};\ Wu3_{Mn} = \frac{1}{100}\frac{s+1}{\frac{s}{5}+1} \tag{26}$$

$$Wu1_{Alt} = Wu2_{Alt} = \frac{1}{100};\ Wu3_{Alt} = \frac{1}{10}\frac{\frac{s}{200}+1}{s+1} \tag{27}$$

To reduce the number of states, and since there are sufficient degrees of freedom in the formulation, the error weight is selected to be a constant. This provides the additional advantage of controlling the roll-off of the filter in a more straightforward manner using only the ideal model, observe in Figure 16 how the filter terms parallel the shape of the ideal model.

$$W_e = 0.1 \tag{28}$$

The final $\mathcal{H}_\infty$ FDI filter has 24 states, 7 inputs ($N1, N2$, EGT, Wf, TAT, Mn and Alt), and 1 output (the fault estimate $\hat{f}$). An $\mathcal{H}_\infty$-norm of 0.84915 is obtained for these interconnection and weights.

Simulation Results

The section concludes with the time simulation of the LTI MIMO and the nonlinear simulation engine models using different closed-loop data sets and a variety of profiles for the high pressure turbine fault, HPT_f.

Figures 17 and 18 provide the input and output data respectively for the two closed-loop flight data sets used for the FDI filter simulation: Flight 1 and Flight 2. These sets are representative of typical cruise regime flights.

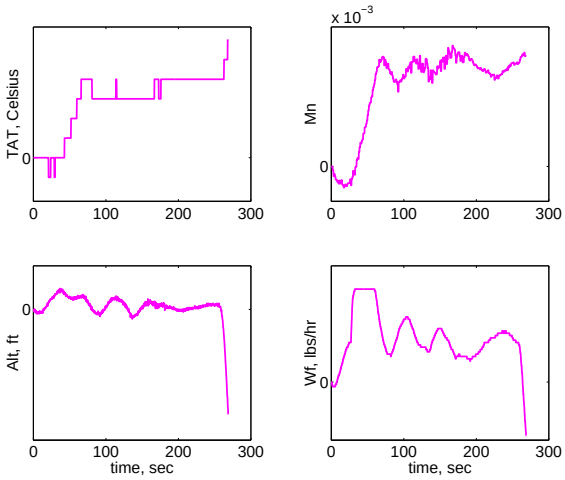

Figure 17. Flight engine data inputs, Flight 2.

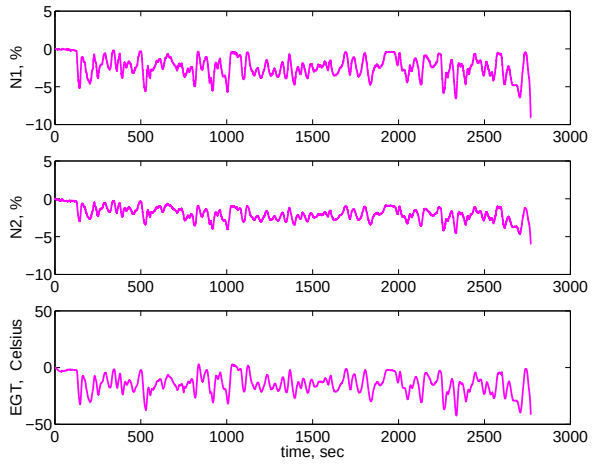

Figure 18. Flight engine data outputs, Flight 1.

The first simulations performed are with respect to the complete (fault plus nominal) LTI MIMO model given in Section 4. Figures 19 and 20 show the simulations for the two flights. It is observed that the fault is adequately detected even for relatively small (incipient) faults and for abrupt faults. The detection time is around 100 seconds, with remarkably good rejection properties.

The last two plots, Figures 21 and 22, show the behavior of the detection filter when applied to the nonlinear simulation model of the engine. It is seen again that the $\mathcal{H}_\infty$ FDI filter is able to identify the high-pressure turbine fault, although there are obvious coupling issues with some of the disturbances. These results indicate the need for using a residual evaluation to provide bounds on the fault estimate in order to improve the false rate.

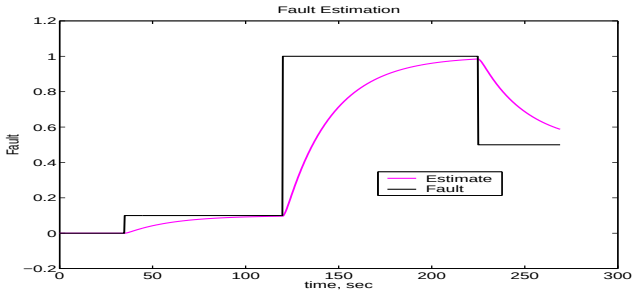

Figure 19. Fault and estimation for LTI MIMO model and Flight 1.

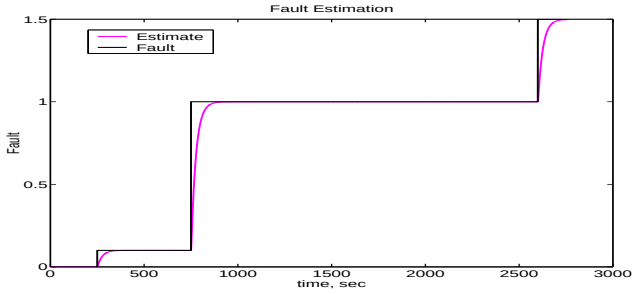

Figure 20. Fault and estimation for LTI MIMO model and Flight 2.

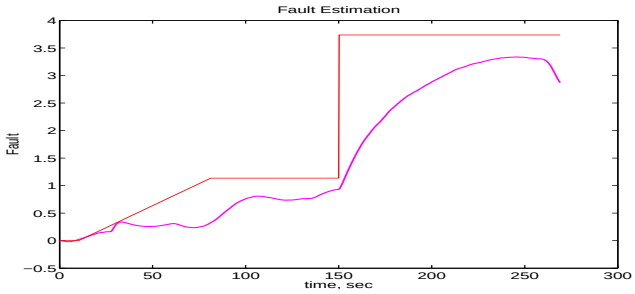

Figure 21. Fault and estimation for nonlinear model and Flight 1.

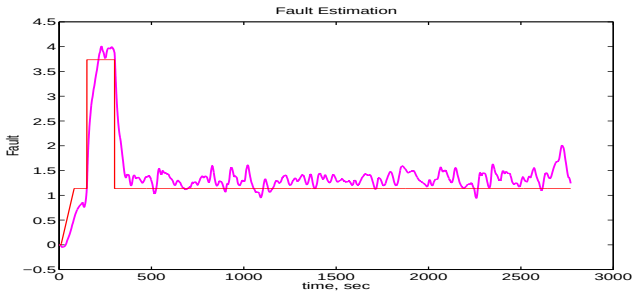

Figure 22. Fault and estimation for nonlinear model and Flight 2.

The need for the residual evaluation stage also arises from the study of the robustness properties of the filter, as measured by its ability to effectively perform on the nonlinear plant. It is noted that there are important differences between the nominal and nonlinear models that prevent the $\mathcal{H}_\infty$-optimization approach from improving. The main differences affecting the performance of the filter arise from variations in the core speed output $N2$. This is unfortunate since the fault to be estimated precisely affects this channel the most and, moreover, the fault propagates in the same direction as the other disturbances which make its estimation more critical in this channel.

This coupling of $N2$ is not surprising since in Section 4 it was noted that although the $N2$ identified model resulted in quite good time domain agreement with the data, the frequency domain analysis indicated some strong phase discrepancies. These phase discrepancies were also indirectly highlighted in the MEM uncertainty analysis where around the region of phase uncertainty (approx. 12 radians) the MEM provided a larger frequency band gain. The MEM test also indicated that the transfer function from the Mach number to the core speed could be the culprit of these problems. This phase uncertainty was addressed through several uncertainty descriptions, mainly additive and input/output multiplicative, and using lead/lag filters to improve the phase while keeping the gain unchanged. Unfortunately, the size of the phase difference prevented the achievement of better robustness of the filter using the nominal MIMO LTI plant.

7. Conclusions

In this paper, we presented an application for robust fault detection and isolation techniques to a Honeywell turbofan engine for the cruise regime. A systematic approach starting from data-driven model identification, model validation, and robust FDI formulation and design was carried out. LTI MIMO parametric models were identified for the nominal and faulty engine cases. We used recent developments on model validation concepts, i.e. the model error model to provide initial characterizations on the modelling uncertainty and to gain understanding of the shortcomings of the nominal identified models. The $\mathcal{H}_\infty$ fault detection and isolation filter obtained has good robustness and performance properties for the LTI MIMO models but it suffers from some disturbance rejection shortcomings for the nonlinear engine model. We are currently investigating performance improvements for the filter.

8. Acknowledgments

The first author would like to thank Honeywell International Inc. for the opportunity to carry out this research as part of a Summer internship at the Vehicle Health Monitoring & Logistics Management Lab in Minneapolis. Special thanks to John Christoffel, Sunil Menon, Önder Uluyol and the rest of the team for their help and interest. We gladly acknowledge the help of Sachi Dash and Hanif Vhora for providing their knowledge and help as the designers of the engine simulation model. Also, we would like to thank Reinelt Wolfgang for the availability of his model error model software.

References

[1] Balas, G.J., Doyle, J.C., Glover, K., Packard, A., and Smith, R. μ-Analysis and Synthesis Toolbox, June 1998.

[2] Chen, J. and Patton, R.J. $\mathcal{H}_\infty$ Formulation and Solution for Robust Fault Diagnosis. In *14th Triennial World Congress of IFAC*, pages 127–132, Beijing,P.R.China, 1999.

[3] Chen, J. and Patton, R.J. *Robust Model-Based Fault Diagnosis for Dynamic Systems*. Kluwer Academic Publishers, 1999.

[4] Chen, J. and Patton, R.J. Standard $\mathcal{H}_\infty$ Filtering Formulation of Robust Fault Detection. In *IFAC SAFEPROCESS*, pages 256–261, Budapest, Hungary, 2000.

[5] Ding, X. and Frank, P.M. An Approach to Robust Residual Generation and Evaluation. In *IEEE Conference on Decision and Control*, Brighton, England, December 1991.

[6] Frisk, E. and Nielsen, L. Robust Residual Generation for Diagnosis Including a Reference Model for Residual Behavior. In *14th Triennial World Congress of IFAC*, pages 55–60, Beijing,P.R.China, 1999.

[7] Gayme, D. and Menon, S. and Ball, C. and Mukavetz, D. and Nwadiogbu, E. Fault Diagnosis in Gas Turbine Engines using Fuzzy Logic. In *2003 IEEE International Conference on Systems, Man, and Cybernetics*, Washington DC, 2003.

[8] Glad, T, Helmersson, A., and Ljung, L. Uncertain lti-models for linear control design of nonlinear systems. In *IEEE Conference on Decision and Control*, Orlando, FL, Aug 2001.

[9] Gorinevsky, D., Dittmar, K., Mylaraswamy, D., and Nwadiogbu, E. Model-Based Diagnostics for an Aircraft Auxiliary Power Unit. In *IEEE Conference on Control Applications*, Glasgow, Scotland, September 2002.

[10] Gorinevsky, D., Nwadiogbu, E., and Mylaraswamy, D. Model-Based Diagnostics for Small-scale Turbomachines. In *IEEE Conference on Decision and Control*, Las Vegas, NV, December 2002.

[11] Isermann, R. Supervision, Fault-Detection and Fault-Diagnosis Methods - An Introduction. *Control Engineering Practice*, 5(5):639–652, 1997.

[12] Kim, K. and Ball, C. and Nwadiogbu, E. Fault Diagnosis in Turbine Engines using Neural Networks Clustering Technique. *2004 American Control Conference*, Boston, MA 2004.

[13] L. Ljung. Model validation and model error modeling. In Wittenmark, B. and Rantzer, A., editors, *The Astrom Symposium on Control*, pages 15–42, Lund, Sweden,

Aug 1999. Studentlitteratur.

[14] Ljung, L. *System Identification Theory for the User*. Information and System Sciences Series. Prentice-Hall, Inc., 1987.

[15] Ljung, L. From Data to Model: A Guided Tour. In *CONTROL'94, IEE Conference on Control*, Warwick, England, Mar 1994.

[16] Ljung, L. Estimating Linear Time-Invariant Models of Nonlinear Time-Varying Systems. *European Journal of Control*, (2-3)(7):203–219, September 2001.

[17] Ljung, L. *System Identification Toolbox User's Guide*. The Mathworks, Inc., July 2002.

[18] Merril, W.C. Sensor Failure Detection for Jet Engines Using Analytical Redundancy. *Journal of Guidance, Control and Dynamics*, (8)(6):673–682, 1985.

[19] Marcos, A., Ganguli, S., and Balas, G.J. Application of $\mathcal{H}_\infty$ Fault Detection and Isolation to a Boeing 747-100/200 Aircraft. In *AIAA Guidance, Navigation, and Control Conference, AIAA-2002-4944*, Monterey, CA, August 2002.

[20] Patton, R.J. and Chen, J. Observer-Based Fault Detection and Isolation: Robustness and Applications. *Control Engineering Practice*, 5(5):671–682, 1997.

[21] Reinelt, W, Garulli, A., and Ljung, L. Comparing different approaches to model error modeling in robust identification. *Automatica*, 38(5):787–803, May 2002.

[22] Reinelt, W, Garulli, A., Ljung, L., Braslavsky, J.H., and Vicino, A. Model error concepts in identification for control. In *IEEE Conference on Decision and Control*, pages 1488–1493, Phoenix, AZ, USA, Dec 1999.

[23] Smith, R., Dullerud, G., Rangan, S., and Poolla, K. Model Validation for Dynamically Uncertain Systems. *Mathematical Modelling of Systems*, 3(1):43–58, January 1997.

[24] Stoustrup, J., Grimble, M.J., and Niemann, H. Design of integrated systems for the control and detection of actuator/sensor faults. *Sensor Review*, 17 (2):138–149, July 1997.

[25] Stoustrup, J. and Niemann, H. Application of an $\mathcal{H}_\infty$ Based FDI and Control Scheme for the Three Tank System. In *IFAC Symposium on Fault Detection, Supervision and Safety for Technical Processes*, pages 268–273, June 2000.

[26] Uluyol, O. and Kim, K. and Menon, S. and Nwadiogbu, E Synergistic Use of Soft Computing Technologies for Fault Detection in Gas Turbine Engines. In *IEEE International Workshop on Soft Computing in Industrial Applications*, Binghamton, NY, 2003.

[27] Zhou, K., Doyle, J.C., and Glover, K. *Robust and Optimal Control*. Prenticel-Hall, Englewood Cliffs, NJ, 1996.

BIOGRAPHY

Andrés Marcos *received his B.S. degree in 1997 from St. Louis University, and his M.S. degree from the University of Minnesota in 2000, both in aerospace engineering. He is currently completing his Ph.D. degree in aerospace engineering from the University of Minnesota, under the direction of Dr. Gary Balas. His research interests include aircraft dynamics and modelling, system identification, modern control techniques, and fault detection & isolation/fault tolerant systems.*

Gary J. Balas *received his B.S. and M.S. degrees in civil and electrical engineering from the University of California, Irvine, and his Ph.D. degree in aeronautics and astronautics from the California Institute of Technology, Pasadena, in 1990. Since 1990, he has been a faculty member in the Department of Aerospace Engineering and Mechanics at the University of Minnesota, Minneapolis. Currently, he is Professor and Co-Director of the Control Science and Dynamical Systems Department at the University of Minnesota. He is a Co-Organizer and developer of the MUSYN Robust Control Short Course and the μ-Analysis and Synthesis Toolbox used with MATLAB and the President of MUSYN, Inc. His research interests include control of flexible structures, model validation and industrial applications of robust control methods.*

Dinkar Mylaraswamy *is a Principal Research Scientist at the Vehicle Health Monitoring & Logistics Management Lab, Honeywell International Inc., since November 1996. He received his Ph.D, in Chemical Engineering from Purdue University in 1996. His research interests include fault diagnosis, condition-based control and modeling. Winner of H.W. Sweatt Award, Honeywell's highest technical award, he is well recognized for his work on the Abnormal Situation Management in petrochemical industry.*